Scientia Iranica D (2011) 18 (6), 1505–1510

Sharif University of Technology

Scientia Iranica

Transactions D: Computer Science & Engineering and Electrical Engineering

www.sciencedirect.com

Invited/Research note

Conductivity imaging of canine body using 3T magnetic resonance electrical impedance tomography (MREIT) system

H.J. Kim [a], Y.T. Kim [a], W.C. Jeong [a], A.S. Minhas [a], C.Y. Lim [b], H.M. Park [b], E.J. Woo [a,*]

[a] *Department of Biomedical Engineering, Kyung Hee University, Yongin, P.O. Box 446-701, Republic of Korea*

[b] *BK21 Basic & Diagnostic Veterinary Specialist Program for Animal Diseases and Department of Veterinary Internal Medicine, Konkuk University, Seoul, P.O. Box 143-701, Republic of Korea*

Received 24 April 2010; revised 20 August 2010; accepted 31 October 2010

KEYWORDS

MREIT;
Magnetic flux density;
Conductivity image;
Canine body;
Harmonic B_z.

Abstract Magnetic Resonance Electrical Impedance Tomography (MREIT) aims to produce cross-sectional images of conductivity distributions inside animal and human subjects. In this study, we validate its feasibility by performing conductivity imaging experiments of post-mortem canine bodies. After clipping the hair of a beagle, we attached four carbon–hydrogel electrodes and placed the dog inside our 3T MRI scanner. We injected the imaging current in the form of short pulses into the imaging area, the timing of which was synchronized with a chosen pulse sequence. By obtaining images of the induced magnetic flux density distributions inside the dog, we reconstructed conductivity images using the single-step harmonic B_z algorithm based on the relationship between conductivity and magnetic flux density. Reconstructed conductivity images of heart, kidney, prostate, and other organs exhibited unique contrast information hardly observed in other imaging modalities. By providing cross-sectional conductivity images with a spatial resolution of a few millimeters, MREIT may deliver unique new diagnostic information in future clinical studies.

1. Introduction

The electrical conductivity of biological tissue is determined by its molecular composition, cellular structure, concentration and mobility of ions in intra-and extra-cellular fluids, temperature and other factors [1–3]. Since it may deliver unique and new diagnostic information related to the physiological and pathological status of the tissue, there have been numerous studies to visualize conductivity distribution inside the human body [4,5].

Magnetic Resonance Electrical Impedance Tomography (MREIT) has been recently proposed for cross-sectional conductivity image reconstructions, with a spatial resolution of a few millimeters [6]. In MREIT, we inject a current into an imaging object through a pair of surface electrodes. The conductivity distribution inside the object affects the internal current pathway, by Ohm's law. The current generates a magnetic field and the induced magnetic flux density is determined by the Biot–Savart law. From MR phase images, we can obtain the induced magnetic flux density data in the form of an image [7–9]. By applying a conductivity image reconstruction algorithm to measured magnetic flux density images subject to multiple imaging currents, we can reconstruct cross-sectional conductivity images of the imaging object.

Incorporating a current source to an existing MRI scanner, the MREIT technique is expected to provide new contrast information. Following the original ideas of MREIT [10–14], there have been numerous studies on its theory [15–17], reconstruction algorithms [18–21] and imaging experiments [22–26]. Post-mortem and *in vivo* animal imaging studies demonstrated that we can produce high-resolution conductivity images of intact animals [25,26]. Though the first trial of human imaging experiments has been lately reported [27], this new imaging method requires further animal studies, focusing on organs of interest, in terms of their conductivity values.

The purpose of this study is to show the potential of the MREIT technique as a new clinically useful bio-imaging

* Corresponding author.
E-mail address: ejwoo@khu.ac.kr (E.J. Woo).

1026-3098 © 2012 Sharif University of Technology. Production and hosting by Elsevier B.V. Open access under CC BY-NC-ND license.
Peer review under responsibility of Sharif University of Technology.

doi:10.1016/j.scient.2011.08.023

modality, through whole body animal imaging experiments. Describing the imaging method, we will show cross-sectional conductivity images of the normal canine chest, upper and lower abdomen and pelvis. We suggest similar imaging studies, using various diseased animal models.

2. Materials and methods

2.1. Conductivity imaging method in MREIT

We assume a three-dimensional imaging object, Ω, with its conductivity distribution, σ, and boundary, $\partial\Omega$. Attaching a pair of surface electrodes, we inject low-frequency current, I, into the object. The injected current spreads throughout the domain, Ω, and induces distributions of current density, $\mathbf{J} = (J_x, J_y, J_z)$, voltage, u, and magnetic flux density, $\mathbf{B} = (B_x, B_y, B_z)$. These are determined by the conductivity distribution, σ, and the boundary geometry of the imaging object, as well as the electrode configuration.

The induced voltage, u, in Ω satisfies the following boundary value problem with the Neumann boundary condition:

$$\begin{aligned} &\nabla \cdot (\sigma(\mathbf{r})\nabla u(\mathbf{r})) = 0 \quad \text{in } \Omega, \\ &-\sigma \nabla u \cdot \mathbf{n} = j \quad \text{on } \partial\Omega, \end{aligned} \tag{1}$$

where $\mathbf{n}$ is the outward unit normal vector on $\partial\Omega$, j is a normal component of the current density on $\partial\Omega$, due to I, and $\mathbf{r} = (x, y, z)$ is a position vector. The current density, $\mathbf{J}$, is given by:

$$\mathbf{J}(\mathbf{r}) = -\sigma(\mathbf{r})\nabla u(\mathbf{r}) \quad \text{in } \Omega. \tag{2}$$

The induced magnetic flux density, $\mathbf{B}$, in Ω can be expressed as:

$$\mathbf{B}(\mathbf{r}) = \mathbf{B}_\Omega(\mathbf{r}) + \mathbf{B}_x(\mathbf{r}) \quad \text{in } \Omega, \tag{3}$$

where $\mathbf{B}_\Omega$ is the magnetic flux density, due to $\mathbf{J}$ in Ω, and $\mathbf{B}_x$ is from currents in external lead wires. From the Biot–Savart law;

$$\mathbf{B}_\Omega(\mathbf{r}) = \frac{\mu_0}{4\pi} \int_\Omega \mathbf{J}(\mathbf{r}') \times \frac{r - r'}{|r - r'|^3} \mathrm{d}\mathbf{r}'. \tag{4}$$

Lee et al. investigated the term $\mathbf{B}_x$ and suggested experimental and also algorithmic ways of minimizing its effects, based on $\nabla^2 \mathbf{B}_x = 0$ in Ω [16]. From the Ampere law, $\mathbf{J}$ in Eq. (2) can be expressed as:

$$\mathbf{J}(\mathbf{r}) = \frac{1}{\mu_0} \nabla \times \mathbf{B}(\mathbf{r}) \quad \text{in } \Omega. \tag{5}$$

Taking the curl of both sides in Eq. (5) and using Eq. (2), we obtain:

$$\nabla^2 \mathbf{B}(\mathbf{r}) = -\mu_0 \nabla u(\mathbf{r}) \times \nabla \sigma(\mathbf{r}) \quad \text{in } \Omega. \tag{6}$$

In the B_z-based MREIT, we measure only B_z using an MRI scanner, where z is the direction of its main magnetic field. Extracting the z-component from Eq. (6), we may find the relation between $\nabla^2 B_z$ and $\nabla\sigma$. To reconstruct an image of σ from measured B_z data sets, Seo et al. and Oh et al. developed the harmonic B_z algorithm, which we used in this paper [18,19].

2.2. Animal preparation

Imaging objects were ten healthy laboratory beagles (four males and six females, 2–3 years old, weighing 8–15 kg). All of them were healthy without a history of any known disease. The dogs were screened for metabolic diseases by complete blood count and serum chemistry analysis. They had no signs of metabolic and neurological problems. To prevent dribbling, we injected 0.1 mg/kg of atrophine sulfate. Ten minutes later, we anesthetized the dog with an intramuscular injection of 0.2 ml/kg Tiletamine and Zolazepam (Zoletil 50, Virbac, France). Twenty minutes later, we sacrificed it with an intravenous injection of 80 mg/kg KCL (Entobar, Hanrim Pharmacy, Korea). After clipping and shaving the hair around a chosen imaging area, we rubbed the region of the electrode attachment using a skin preparation gel (D.O. Weaver and Co., USA). This procedure was approved by the Institutional Animal Care and Use Committee (IACUC) of Konkuk University, Seoul, Korea.

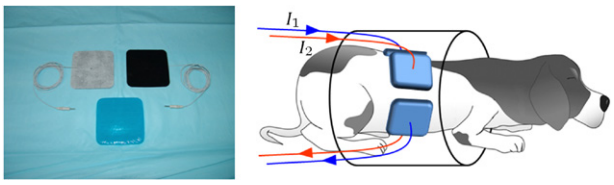

Figure 1: Carbon–hydrogel electrodes for current injection and MREIT imaging setup inside the bore.

2.3. Imaging experiment

We attached four carbon–hydrogel electrodes (HUREV Co. Ltd., Korea) around the imaging area (Figure 1). The size of each electrode was $80 \times 80 \times 5.76$ mm^3. By using large electrodes with a wide coverage of the circumference, we tried to induce a more uniform internal current density distribution. We placed the animal inside the bore of our 3T MRI scanner (Magnum 3, Medinus Co. Ltd., Korea). We injected currents in two mutually orthogonal directions between two pairs of electrodes facing each other. The injection current amplitude ranged from 25 to 35 mA. We adopted the injection current nonlinear encoding (ICNE) pulse sequence [28]. The imaging parameters were as follows:

1. Chest imaging: TR/TE = 1000/30 ms, FOV = 240×240 mm^2, matrix size = 128×128, slicethickness = 5 mm, number of slices = 8, NEX = 24 and total imaging time = 200 min.
2. Abdomen imaging: TR/TE = 1200/30 ms, FOV = 280×280 mm^2, matrix size = 128×128, slice thickness = 4 mm, number of slices = 8, NEX = 10 and total imaging time = 100 min.
3. Pelvis imaging: TR/TE = 1000/30 ms, FOV = 220×220 mm^2, matrix size = 128×128, slice thickness = 4 mm, number of slices = 8, NEX = 16 and total imaging time = 120 min.

2.4. Conductivity image reconstruction

We used CoReHA (conductivity reconstructor using harmonic algorithms), which is an integrated software package for MREIT [29,30]. It provides GUI-based functions for all data processing routines needed to produce conductivity images from measured k-space data sets. We used the single-step harmonic B_z algorithm implemented in CoReHA for multi-slice conductivity image reconstructions [31]. All conductivity images presented in this paper should be interpreted as scaled conductivity images, providing only contrast information.

3. Results

3.1. Chest imaging

Figure 2 shows images of a canine chest. The reconstructed conductivity image reveals conductivity contrasts among the

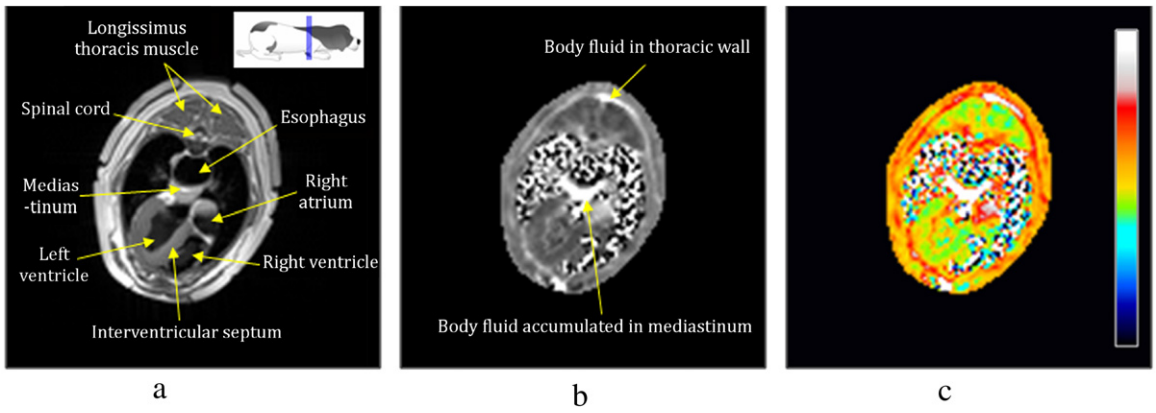

Figure 2: Chest imaging: (a) MR magnitude image; (b) reconstructed conductivity image; and (c) color-coded conductivity image. Conductivity images inside the lungs show spurious spike noise due to the MR signal void there.

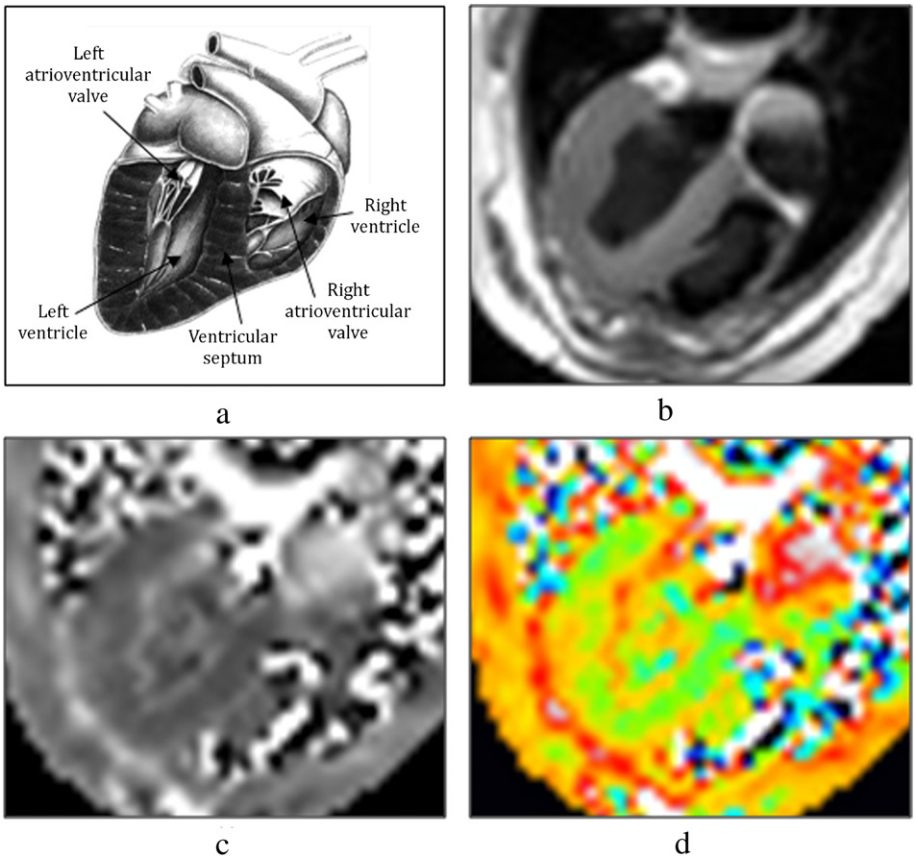

Figure 3: Magnified images of the heart: (a) Anatomy of the heart; (b) MR magnitude image; (c) reconstructed conductivity image; and (d) color-coded conductivity image. Conductivity images distinguish the ventricle, ventricular septum and myocardium.

heart, longissimus thoracis muscle, and thoracic wall. Since MR signals from the lungs are weak, conductivity images of the lungs show peculiar noise patterns. The enlarged conductivity image of the heart (Figure 3) well distinguishes the heart structure, including the ventricle, ventricular septum and myocardium.

3.2. Abdomen imaging

Figure 4 shows images of a canine upper abdomen. Conductivity images reveal different organs, including the liver, stomach, gallbladder and blood vessels. Figure 5 shows images of a canine lower abdomen. Conductivity images distinguish organs in the lower abdomen, including the spinal cord, peritoneal cavity, kidney, liver, large and small intestines, spleen and stomach. The peritoneal cavity, which mainly consists of conductive fluids, shows a high conductivity value. The internal medulla of the kidney and the urethra appear to be significantly more conductive than the cortex of the kidney.

3.3. Pelvis imaging

Figure 6 shows images of a canine pelvis. Conductivity images exhibit different contrasts for the prostate, sacrum,

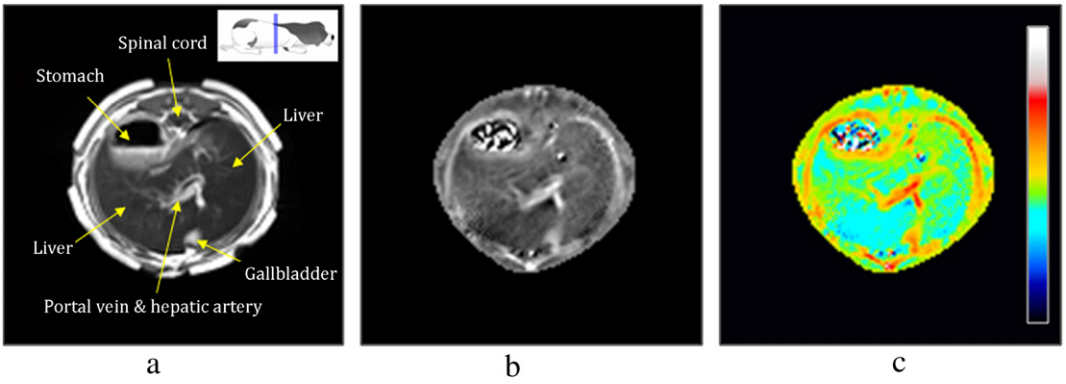

Figure 4: Upper abdomen imaging: (a) MR magnitude image; (b) reconstructed conductivity image; and (c) color-coded conductivity image.

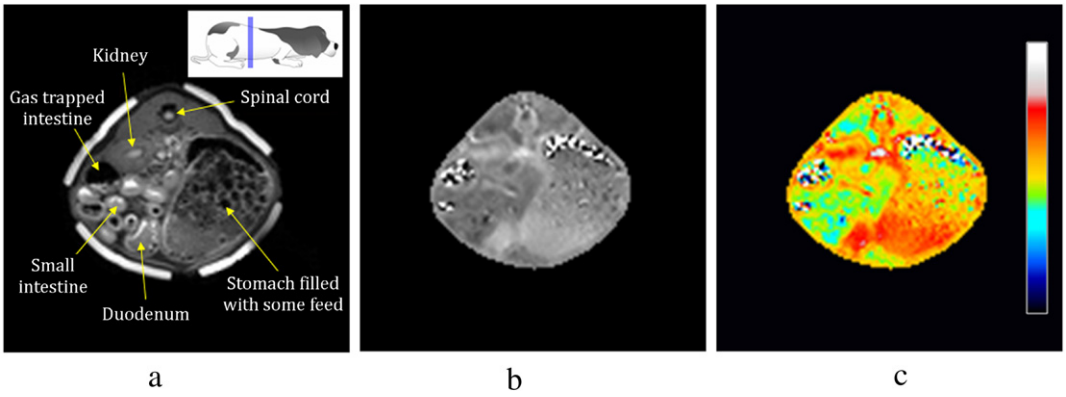

Figure 5: Lower abdomen imaging: (a) MR magnitude image; (b) reconstructed conductivity image; and (c) color-coded conductivity image.

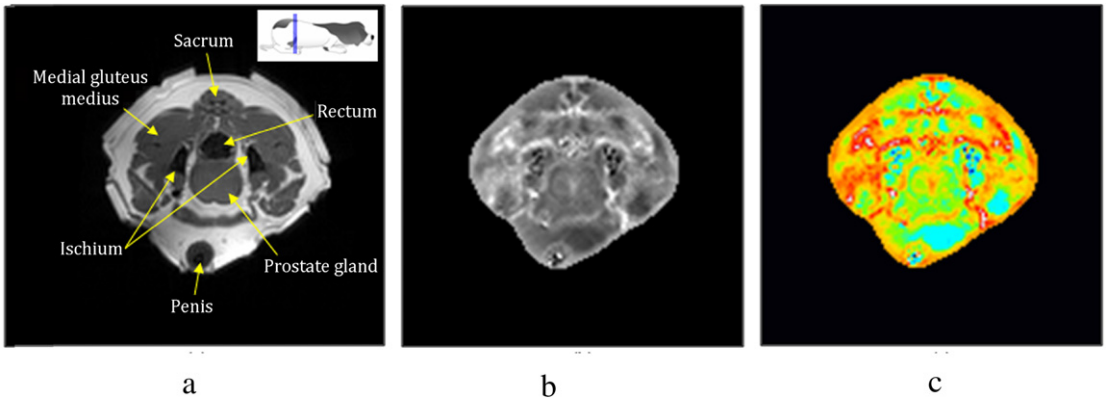

Figure 6: Pelvis imaging: (a) MR magnitude image; (b) reconstructed conductivity image; and (c) color-coded conductivity image.

rectum and surrounding muscles. Figure 7 shows enlarged images of the prostate. Compared with the MR magnitude image of the prostate, the corresponding conductivity image shows a clear contrast between the central and peripheral zones, which are closely related to prostate cancer and benign prostatic hyperplasia.

4. Discussion and conclusion

MREIT has now reached the stage of animal and human experiments. To support its clinical significance, we should demonstrate that the conductivity image provides meaningful diagnostic information that is not available from other imaging modalities. This requires accumulated experience and knowledge on how to interpret a conductivity image in relation to the anatomy and pathology of a specific tissue and organ. Conductivity images shown in this paper indicate that numerous tissues and organs in the canine chest, abdomen, and pelvis are distinguishable in a different way compared with MR images.

MR imaging of the chest is known to be troublesome because of physical and physiological factors such as low proton density, susceptibility effects, respiratory movements, and cardiac and vascular pulsations [32,33]. There are several MR strategies to overcome these problems, and some are based on a standard ^{1}H MRI aimed at increasing the SNR of lung parenchyma [34–36]. Equipped with a different contrast mechanism, MREIT imaging of the chest will be supplementary to the conventional

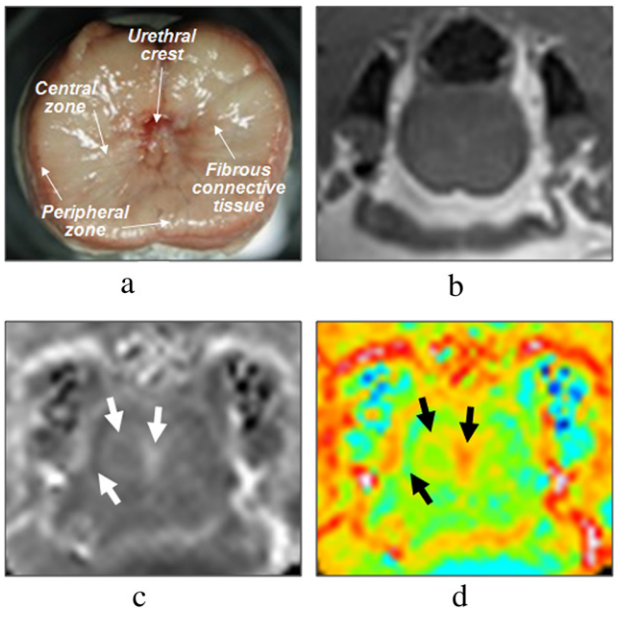

Figure 7: Magnified images of the prostate: (a) Anatomical structure (www.ultrasound.med.umich.edu); (b) MR magnitude image; (c) reconstructed conductivity image; and (d) color-coded conductivity image. Conductivity images distinguish the central and peripheral zones, which are closely related to prostate cancer and benign prostatic hyperplasia. Arrows indicate the canine prostate structure.

MR imaging. Lung diseases, such as pneumonia and edema, are expected to be clearly distinguishable in a conductivity image, primarily due to enhanced conductivity values associated with them. Electrical conductivity imaging of the heart could be another long-term research goal, with a significant influence on the electrophysiology of the heart. Conductivity imaging of the breast has been of special interest as an alternative or supplementary diagnostic method to X-ray mammography. MREIT imaging of the breast is worth further investigation.

There are numerous organs in the abdomen. We may expect conductivity contrasts in those organs related to gastric juices, blood and water content, inflammation, pathology of tissues, and so on. Organs of special interest may include the liver, gallbladder, kidney, spleen, stomach, and small and large intestines. For the pelvic region, conductivity imaging of the prostate is particularly promising for classification of prostate cancer and benign prostatic hyperplasia [37].

It is premature to affirm that MREIT is of clinical value. Most of all, imaging experiments of various diseased animal models must be undertaken to promote clinical trials. We should identify clinical problems where conductivity images may add a significant diagnostic value. These experimental validation studies demand technical progress in terms of specialized MREIT pulse sequences and RF coil. The spin echo pulse sequence has been widely used in MREIT and produces postmortem and *in vivo* conductivity images of animal and human subjects [25–27,30]. The image quality depends on the SNR of the measured magnetic flux density image. In order to reduce scan time and current amplitude, while keeping image quality, we are developing a fast pulse sequence for MREIT. MREIT must also be accompanied by recent technical advancements in general MRI technology. Providing cross-sectional conductivity images with a spatial resolution of a few millimeters, we expect MREIT to deliver unique diagnostic information.

Acknowledgment

This work was supported by the National Research Foundation of Korea (NRF) grant funded by the Korea government (MEST) (No. 20100018275).

References

[1] Geddes, L.A. and Baker, L.E. "The specific resistance of biological material: a compendium of data for the biomedical engineer and physiologist", *Med. Biol. Eng.*, 5, pp. 271–293 (1967).
[2] Gabriel, S., Lau, R.W. and Gabriel, C. "The dielectric properties of biological tissues: II. Measurements in the frequency range 10 Hz to 20 GHz", *Phys. Med. Biol.*, 44, pp. 2251–2269 (1996).
[3] Grimnes, S. and Martinsen, O.G., *Bioimpedance and Bioelectricity Basics*, Academic Press, London, UK pp. 93–124 (2000).
[4] Metherall, P., Barber, D.C., Smallwood, R.H. and Brown, B.H. "Three-dimensional electrical impedance tomography", *Nature*, 380, pp. 509–512 (1996).
[5] Holder, D., *Electrical Impedance Tomography: Methods, History and Applications*, IOP Publishing, Bristol (2005).
[6] Woo, E.J. and Seo, J.K. "Magnetic resonance electrical impedance tomography (MREIT) for high-resolution conductivity imaging", *Physiol. Meas.*, 29, pp. R1–26 (2008).
[7] Joy, M.L.G., Scott, G.C. and Henkelman, R.M. "In vivo detection of applied electric currents by magnetic resonance imaging", *Magn. Reson. Imaging.*, 7, pp. 89–94 (1989).
[8] Scott, G.C., Joy, M.L.G., Armstrong, R.L. and Henkelman, R.M. "Measurement of nonuniform current density by magnetic resonance", *IEEE Trans. Med. Imag.*, 10, pp. 362–374 (1991).
[9] Scott, G.C., Joy, M.L.G., Armstrong, R.L. and Hankelman, R.M. "Sensitivity of magnetic resonance current density imaging", *J. Magn. Reson.*, 97, pp. 235–254 (1992).
[10] Zhang, N. "Electrical impedance tomography based on current density imaging", Toronto, Canada, MS Thesis, Dept. of Elec. Eng. (1992).
[11] Woo, E.J., Lee, S.Y. and Mun, C.W. "Impedance tomography using internal current density distribution measured by nuclear magnetic resonance", *SPIE*, 2299, pp. 377–385 (1994).
[12] Birgul, O. and Ider, Y.Z. "Electrical impedance tomography using the magnetic field generated by injected currents", *Proc. 18th Ann. Int. Conf. IEEE EMBS*, pp. 784–785 (1996).
[13] Ider, Y.Z. and Birgul, O. "Use of the magnetic field generated by the internal distribution of injected currents for electrical impedance tomography (MR-EIT)", *Elektrik*, 6, pp. 215–225 (1998).
[14] Kwon, O., Woo, E.J., Yoon, J.R. and Seo, J.K. "Magnetic resonance electrical impedance tomography (MREIT): simulation study of J-substitution algorithm", *IEEE Trans. Biomed. Eng.*, 49, pp. 160–167 (2002).
[15] Ider, Y.Z., Onart, S. and Lionheart, W.R.B. "Uniqueness and reconstruction in magnetic resonance electrical impedance tomography (MREIT)", *Physiol. Meas.*, 24, pp. 591–604 (2003).
[16] Lee, B.I., Oh, S.H., Woo, E.J., Lee, S.Y., Cho, M.H., Kwon, O., Seo, J.K., Lee, J.Y. and Baek, W.S. "Three-dimensional forward solver and its performance analysis in magnetic resonance electrical impedance tomography (MREIT) using recessed electrodes", *Phys. Med. Biol.*, 48, pp. 1971–1986 (2003).
[17] Kwon, O., Pyo, H.C., Seo, J.K. and Woo, E.J. "Mathematical framework for B_z-based MREIT model in electrical impedance imaging", *Comp. Math. Appl.*, 51, pp. 817–828 (2006).
[18] Oh, S.H., Lee, B.I., Woo, E.J., Lee, S.Y., Cho, M.H., Kwon, O. and Seo, J.K. "Conductivity and current density image reconstruction using harmonic B_z algorithm in magnetic resonance electrical impedance tomography", *Phys. Med. Biol.*, 48, pp. 3101–3116 (2003).
[19] Seo, J.K., Yoon, J.R., Woo, E.J. and Kwon, O. "Reconstruction of conductivity and current density images using only one component of magnetic field measurements", *IEEE Trans. Biomed. Eng.*, 50, pp. 1121–1124 (2003).
[20] Park, C., Kwon, O., Woo, E.J. and Seo, J.K. "Electrical conductivity imaging using gradient B_z decomposition algorithm in magnetic resonance electrical impedance tomography (MREIT)", *IEEE Trans. Med. Imag.*, 23, pp. 388–394 (2003).
[21] Gao, N., Zhu, S.A. and He, B. "New magnetic resonance electrical impedance tomography (MREIT) algorithm: the RSM–MREIT algorithm with applications to estimation of human head conductivity", *Phys. Med. Biol.*, 51, pp. 3067–3083 (2006).
[22] Birgul, O., Eyuboglu, B.M. and Ider, Y.Z. "Experimental results for 2D magnetic resonance electrical impedance tomography (MREIT) using magnetic flux density in one direction", *Phys. Med. Biol.*, 48, pp. 3485–3504 (2003).
[23] Oh, S.H., Lee, B.I., Park, T.S., Lee, S.Y., Woo, E.J., Cho, M.H., Kwon, O. and Seo, J.K. "Magnetic resonance electrical impedance tomography at 3 Tesla field strength", *Mag. Reson. Med.*, 51, pp. 1292–1296 (2004).

[24] Hamamura, M.J., Muftuler, L.T., Birgul, O. and Nalcioglu, O. "Measurement of ion diffusion using magnetic resonance electrical impedance tomography", *Phys. Med. Biol.*, 51, pp. 2753–2762 (2006).
[25] Kim, H.J., Lee, B.I., Cho, Y., Kim, Y.T., Kang, B.T., Park, H.M., Lee, S.Y., Seo, J.K. and Woo, E.J. "Conductivity imaging of canine brain using a 3 T MREIT system: postmortem experiments", *Physiol. Meas.*, 28, pp. 1341–1353 (2007).
[26] Kim, H.J., Oh, T.I., Kim, Y.T., Lee, B.I., Woo, E.J., Seo, J.K., Lee, S.Y., Kwon, O., Park, C., Kang, B.T. and Park, H.M. "In vivo electrical conductivity imaging of a canine brain using a 3T MREIT system", *Physiol. Meas.*, 29, pp. 1145–1155 (2008).
[27] Kim, H.J., Kim, Y.T., Minhas, A.S., Jeong, W.C., Woo, E.J., Seo, J.K. and Kwon, O.J. "In vivo high-resolution conductivity imaging of the human leg using MREIT: the first human experiment", *IEEE Trans. Med. Imag.*, 28, pp. 1681–1687 (2009).
[28] Park, C., Lee, B.I., Kwon, O. and Woo, E.J. "Measurement of induced magnetic flux density using injection current nonlinear encoding (ICNE) in MREIT", *Physiol. Meas.*, 28, pp. 117–127 (2007).
[29] Jeon, K., Kim, H.J., Lee, C.O., Woo, E.J. and Seo, J.K. "CoReHA: conductivity reconstructor using harmonic algorithms for magnetic resonance electrical impedance tomography (MREIT)", *J. Biomed. Eng. Res.*, 30, pp. 279–287 (2009).
[30] Jeon, K., Minhas, A.S., Kim, Y.T., Jeong, W.C., Kim, H.J., Kang, B.T., Park, H.M., Lee, C.O., Seo, J.K. and Woo, E.J. "MREIT conductivity imaging of postmortem canine abdomen using CoReHA", *Physiol. Meas.*, 30, pp. 957–966 (2009).
[31] Seo, J.K., Kim, S.W., Kim, S., Liu, J.J., Woo, E.J., Jeon, K. and Lee, C.O. "Local harmonic B_z algorithm with domain decomposition in MREIT: computer simulation study", *IEEE Trans. Med. Imag.*, 27, pp. 1754–1761 (2008).
[32] Leutner, C. and Schild, H. "MRI of the lung parenchyma", *RoFo*, 173, pp. 168–175 (2001).
[33] Bergin, C.J., Noll, D.C., Pauly, J.M., Glover, G.H. and Macovski, A. "MR imaging of lung parenchyma: a solution to susceptibility", *Radiology*, 183, pp. 673–676 (1992).
[34] Mayo, J.R., MacKay, A. and Muller, N.L. "MR imaging of the lungs: value of short TE spin-echo pulse sequences", *Am. J. Roentgenol.*, 159, pp. 951–956 (1992).
[35] Levin, D.L., Chen, Q., Zhang, M., Edelman, R.R. and Hatabu, H. "Evaluation of regional pulmonary perfusion using ultrafast magnetic resonance imaging", *Magn. Reson. Med.*, 46, pp. 166–171 (2001).
[36] Mai, V.M., Knight-Scott, J., Edelman, R.R., Chen, Q., Keilholz-George, S. and Berr, S.S. "^{1}H magnetic resonance imaging of human lung using inversion recovery turbo spin echo", *J. Magn. Reson. Imaging.*, 11, pp. 616–621 (2000).
[37] Engelbrecht, M.R., Huisman, H.J., Laheij, R.J., Jager, G.J., van Leenders, G.J., Hulsbergen-Van De Kaa, C.A., de la Rosette, J.J., Blickman, J.G. and Barentsz, J.O. "Discrimination of prostate cancer from normal peripheral zone and central gland tissue by using dynamic contrast-enhanced MR imaging", *Radiology*, 229, pp. 248–254 (2003).

Biographies of the respected authors, **Hyung Joong Kim**, **Young Tae Kim**, **Woo Chul Jeong**, **Atul S. Minhas**, **Chae Young Lim**, and **Hee Myung Park**, were not available at the time of publication.

Eung Je Woo received B.S. and M.S. degrees in Electronic Engineering from Seoul National University in 1983 and 1985, respectively. He joined the BME group at the University of Wisconsin–Madison in 1986 and received his Ph.D. degree in 1990. From 1990 to 1999, he was with the BME department at Konkuk University as Assistant and Associate. In 1999, he moved to Kyung Hee University as Professor, where he has been teaching bioinstrumentation and doing research in electrical impedance imaging, the modeling of bioelectromagnetism, and instrumentation. He is a life-time member of the KOSOMBE and a senior member of the IEEE. In 2010, he was elected as an AdCom member of the IEEE EMBS, representing the Asia–Pacific region. He was Chairman of the scientific program committee for the WC2006. For the IEEE EMBC09, he served as Co-chairman of the biomedical imaging and image processing theme.